



Electron Transport Modeling in Biological Tissues: From Water to DNA

Mario E. Alcocer-Ávila¹, Michele A. Quinto², Juan M. Monti²,
Roberto D. Rivarola², and Christophe Champion¹(✉)

¹ Université de Bordeaux, CNRS, CEA, CELIA (Centre Lasers Intenses et Applications), UMR 5107, 33405 Talence, France
christophe.champion@u-bordeaux.fr

² Instituto de Física Rosario, CONICET – Universidad Nacional de Rosario, S2000 EKF Rosario, Argentina

Abstract. A proper and reliable description of charged particles interactions in the biological matter remains a critical aspect of radiation research. All the more so when new and better methods for treating cancer through the use of ionizing radiation are emerging on the horizon such as targeted alpha therapy. In this context, Monte Carlo track-structure codes are extremely useful tools to study radiation-induced effects at the atomic scale. In the present work, we review the latest version of CELLDOSE, a *homemade* Monte Carlo track-structure code devoted to electron dosimetry in biological matter. We report here some recent results concerning the stopping power and penetration range of electrons in water and DNA for impact energies ranging from 10 eV to 10 keV.

1 Introduction

A complete and accurate description of charged particles' interactions with matter at the nanometric scale is essential for understanding the radio-induced biological effects such as cellular death and chromosomal aberration induction. Computer simulations, particularly those based on Monte Carlo (MC) methods, are a very powerful tool in this field and have been used for decades to tackle particle transport problems. MC radiation transport codes can be grouped into two categories depending on how the particles are tracked: condensed-history (MCCH) codes and track-structure (MCTS) codes. In MCCH codes, also known as general-purpose MC codes, a particle's path is divided into discrete steps, each step encompassing a large number of collision processes and taking into account their combined effects by means of multiple scattering theories. This allows to determine the energy losses and angular changes in the direction of the particle at the end of the step [1]. Some examples of general-purpose MC codes are PENELOPE, MCNP, Geant4, and FLUKA. Although MCCH codes have the obvious advantage of reducing computation time and provide results accurate enough for most applications in radiation therapy, they have also important

shortcomings, especially when dealing with very small geometries or low-energy transfers [2,3]. Therefore, only MCTS codes are appropriate for microdosimetry applications and remain the only tools able to reproduce in detail the energy deposit pattern in small biological structures such as cell nucleus or DNA subunits (nucleobase, sugar-phosphate backbone) [4]. Contrary to MCCH codes, MCTS codes follow both the primary and the secondary particles in an event-by-event manner, until their energy falls below a cutoff value. Track-structure simulations consist in a series of random samplings, which first determine the distance traveled by the particle, then the type of interaction taking place at the point of arrival and finally the full kinematics of the secondary particles created. To properly simulate the transport of particles in a given medium, MCTS codes require total and differential cross sections for describing the various particle-induced interactions as input data. Most of the time, these cross sections are obtained using a combination of experimental data and theoretical models. It is worth noting that, in the end, the effectiveness and reliability of the code will depend on how accurate and complete the cross sections database is.

The preferred medium for the simulations in most of the existing MCTS codes designed for applications in radiobiology and medical physics is water, since it has often been considered a good surrogate for tissue. A few codes have also included models which allow to explore in more detail the damage to DNA [5,6]. A summary of some well-known MCTS codes and their relevant features may be found in [1,2].

The purpose of this paper is to review the latest version of CELLDOSE, an *homemade* MCTS code for electron dosimetry in biological matter [7]. We present some of our results and discuss the ongoing work devoted to extend the code's capabilities. In Sect. 2, we summarize the main features of CELLDOSE and we provide the theoretical framework used to describe the biological media and the physical processes considered in the code, concluding with a general outline of the future developments. In Sect. 3, we present our calculations regarding the stopping power and the penetration range for electrons in water and DNA and compare them with values found in the literature.

2 CELLDOSE

CELLDOSE is an MCTS code developed in the C++ programming language. In its current version, it is able to simulate the full slowing-down histories of electrons and positrons in gaseous and liquid water, as well as in DNA. The underlying physics of CELLDOSE—needed to describe the elastic as well as the inelastic electron-induced processes—refers to several theoretical models independently developed and mostly within the quantum-mechanical framework. For more details, we refer the reader to some of our previous studies where the ionization treatment for electrons in water is detailed [8], where the elastic scattering of electrons and positrons has been studied in liquid and gaseous water [9], and finally to [10] where the ionization of DNA subunits was investigated. All these models were summarized in [11] and implemented into a *homemade*

Monte Code track-structure code—called EPOTRAN—devoted to electron and positron transport in water for impact energies ranging from 1 MeV down to a predefined energy cutoff of 7.4 eV (i.e. the water excitation threshold) [12]. Thus, CELLDOSE may be seen as a dosimetric extension of EPOTRAN whose current extension includes newly studied electron–DNA interactions. In this context, CELLDOSE has been used previously to assess the electron dose distribution for several radionuclides in simple geometries [7, 13] as well as in more complex environments [14].

2.1 Description of the Biological Medium: From Water to DNA

In CELLDOSE, the water target is described following the quantum approach proposed by Moccia for water vapor [15]. The ten bound electrons of the water target are distributed in five molecular orbitals ($j = 5$), which are constructed from a linear combination of atomic orbitals in a self-consistent field. Each molecular orbital wave function is developed in terms of Slater-type-orbital functions centered on the oxygen nucleus. According to this description, the molecular orbital wave functions are written as

$$\psi_j(r) = \sum_{k=1}^{N_j} a_{jk} \phi_{n_{jk} l_{jk} m_{jk}}^{\xi_{jk}}(r) \quad (1)$$

where N_j is the number of Slater atomic orbitals $\phi_{n_{jk} l_{jk} m_{jk}}^{\xi_{jk}}$ and a_{jk} is the corresponding weight. The atomic components are written as

$$\phi_{n_{jk} l_{jk} m_{jk}}^{\xi_{jk}}(r) = R_{n_{jk}}^{\xi_{jk}}(r) S_{l_{jk} m_{jk}}(\hat{r}), \quad (2)$$

with the radial part given by

$$R_{n_{jk}}^{\xi_{jk}}(r) = \frac{(2\xi_{jk})^{2n_{jk}+1/2}}{\sqrt{2n_{jk}!}} r^{n_{jk}-1} e^{-\xi_{jk}r}, \quad (3)$$

and the angular part, expressed by means of real spherical harmonics, is given by:

$$\left\{ \begin{array}{l} \text{if } m_{jk} \neq 0 : S_{l_{jk} m_{jk}}(\hat{r}) = \left(\frac{m_{jk}}{2|m_{jk}|} \right)^{1/2} \\ \quad \times \left\{ Y_{l_{jk} -|m_{jk}|}(\hat{r}) + (-1)^{m_{jk}} \left(\frac{m_{jk}}{|m_{jk}|} \right) Y_{l_{jk} |m_{jk}|}(\hat{r}) \right\}, \\ \text{if } m_{jk} = 0 : S_{l_{jk} 0}(\hat{r}) = Y_{l_{jk} 0}(\hat{r}). \end{array} \right. \quad (4)$$

All the necessary coefficients and quantum numbers are reported in [15].

DNA modeling follows a similar *ab initio* approach in which each component (i.e., nucleobase or sugar-phosphate backbone unit) is described via N molecular subshell wave functions similar to (1); $N = 35, 29, 39, 33, 29$ and 48 for adenine (A), cytosine (C), guanine (G), thymine (T), uracil (U), and sugar-phosphate backbone unit (SP), respectively. Each molecular subshell wave function is expressed as a linear combination of atomic wave functions corresponding

to the different atomic components: H_{1s} , C_{1s} , C_{2s} , C_{2p} , N_{1s} , N_{2s} , N_{2p} , O_{1s} , O_{2s} , O_{2p} , P_{1s} , P_{2s} , P_{3s} , P_{2p} , and P_{3p} . Total-energy calculations for all targets were performed in the gas phase with the Gaussian 09 software at the RHF/3-21G level of theory [16]. The computed ionization energies of the occupied molecular orbitals of the targets were scaled so that the ionization energy of their HOMO coincides with the experimental values found in the literature. For each molecular orbital j , the effective number of electrons relative to the atomic component k was derived from a standard Mulliken population analysis and their sum for every occupied molecular orbital is very close to 2, since only atomic shells with very small population were discarded. More details about this model are provided in [17]. Besides, to get insight into the real energy deposit cartography induced by charged particles impact in the biological medium, a DNA molecule composed of a nucleobase-pair plus two SP groups has been considered. Additionally, to fit the realistic composition of living cells, we used the nucleobase repartition percentages reported by Tan et al. [18], namely, 58% (A-T) (adenine–thymine base pair) and 42% (C-G) (cytosine–guanine base pair). Thus, by using the respective molar mass of each DNA component, viz. $M_A = 135.14 \text{ g mol}^{-1}$, $M_T = 126.12 \text{ g mol}^{-1}$, $M_C = 111.11 \text{ g mol}^{-1}$, $M_G = 151.14 \text{ g mol}^{-1}$ and $M_{SP} = 180 \text{ g mol}^{-1}$, the following mass percentages were obtained: A (12.6%), T (11.8%), C (7.5%), G (10.2%) and SP group (57.9%). However, this description corresponds to dry DNA. In order to obtain an even more realistic biological medium, hydrated DNA was simulated by adding 18 water molecules per nucleotide, which modified the mass percentages as follows: A (8.3%), T (7.7%), C (4.9%), G (6.7%), SP group (38.1%), and water (34.3%). This is consistent with the suggestion made by Birnie et al. [19] who estimated that the total amount of water associated with DNA was of the order of 50 moles per mole of nucleotide, in order to get the expected density of 1.29 g cm^{-3} .

Irrespective of the biomolecular targets investigated, CELLDOSE is based on a cross section database, which refers to *isolated* molecules and to living matter components in *vapor* state. In this context, the present work clearly differs from existing studies on *condensed* matter (water or DNA), where the energy-loss function of realistic biological components was extracted from experimental data and interpolated for use in cross section calculations (see for example [20] and the recent series of works by Abril and coworkers [21,22] and Emfietzoglou et al. [23]) or developed within the independent atom model framework [24]. However, whether it is for water or DNA, the available data—cross sections as well as macroscopic outcomes like ranges and stopping power—are exclusively measured in vapor phase and comparisons with the liquid homologous have been only rarely reported. Consequently, a *vapor-based* approach is chosen here in order to check the suitability of our theoretical models, although comparisons with existing condensed matter models are presented in the Results section of this manuscript. Nevertheless, the theoretical models described in the following section report some information about the extrapolations performed for treating the liquid water phase, in particular for modeling the elastic scattering process [9] and the electron-induced ionization [25].

2.2 Interactions and Cross Sections

CELLDOSE implements a set of theoretical cross sections calculated within the quantum-mechanical framework, using the partial-wave method. The following interactions are taken into account in the code: elastic scattering of the incident particle; ionization and electronic excitation of the target molecule; and Positronium formation, when the primary particle is a positron. We report hereafter some details on the theoretical treatment of electron-induced interactions in water by considering—in some cases—the vapor and liquid environment specificities.

Elastic Scattering. When the selected interaction is elastic scattering, the singly differential cross sections are sampled in order to determine the scattering direction at the electron incident energy E_{inc} , which remains almost unchanged because the energy transfer induced during this process is very small (of the order of meV) [12].

The perturbation potential of the water molecule can be approximated by a spherically symmetric potential $V(r)$ composed of three different terms: the static contribution V_{st} , the correlation-polarization term V_{cp} , and the exchange term V_{ex} . Thus, we can write:

$$\begin{cases} V(r) = V_{\text{st}}(r) + V_{\text{cp}}(r) + V_{\text{ex}}(r) & \text{for electrons,} \\ V(r) = -V_{\text{st}}(r) + V_{\text{cp}}(r) & \text{for positrons.} \end{cases} \quad (5)$$

As we mentioned before, for water *vapor* the description of the water molecule provided by Moccia [15] was used. The static potential $V_{\text{st}}(r)$ was numerically calculated from each target molecular wave function by using the spherical average approximation and is expressed as

$$V_{\text{st}}(r) = \sum_{j=1}^{N_{\text{orb}}} [V_{\text{st}}^j(r)]_{\text{elec}} + [V_{\text{st}}(r)]_{\text{ion}}, \quad (6)$$

where $[V_{\text{st}}^j(r)]_{\text{elec}}$ and $[V_{\text{st}}(r)]_{\text{ion}}$ refer to the electronic and ionic target contribution to the static potential, respectively.

For *liquid* water, the molecular wave functions can only be obtained by theoretical calculations performed in the Dynamic Molecular framework, which rapidly becomes extremely computer time-consuming. To overcome this limitation, the static potential for liquid water has been deduced from the experimental electron density reported by Neufeind et al. [26]. This latter was then fitted and analytically expressed as [9]:

$$\rho_N(r) = \frac{1}{4\pi} \left(a_1 e^{-r/b_1} + a_2 r e^{-r/b_2} \right), \quad (7)$$

what leads to a static potential given by

$$V_N(r) = -\frac{1}{r} [a_1 b_1^2 (r + 2b_1) e^{-r/b_1} + a_2 b_2^2 (r^2 + 4b_2 r + 6b_2^2) e^{-r/b_2} + (2\delta - 2)], \quad (8)$$

where $a_1 = 4411$ a.u., $a_2 = 120.435$ a.u., $b_1 = 0.06046$ a.u., $b_2 = 0.3248$ a.u. and the parameter δ is expressed as

$$\delta = \begin{cases} \frac{r}{R_{\text{OH}}} & \text{for } r \leq R_{\text{OH}} \\ 1 & \text{for } r > R_{\text{OH}}, \end{cases} \quad (9)$$

with $R_{\text{OH}} = 1.8336$ a.u. for the water molecule in liquid phase [27,28]. The correlation-polarization contribution is based on the recommendations of Salvat [29] and is given by

$$V_{\text{cp}}(r) = \begin{cases} \max\{V_{\text{corr}}(r), V_{\text{p}}(r)\} & \text{for } r < r_{\text{cr}} \\ V_{\text{p}}(r) & \text{for } r > r_{\text{cr}}, \end{cases} \quad (10)$$

where r_{cr} is defined as the outer radius at which $V_{\text{p}}(r)$ and $V_{\text{corr}}(r)$ cross. The polarization potential $V_{\text{p}}(r)$ is the same for electrons and positrons and is given by

$$V_{\text{p}}(r) = -\frac{\alpha_{\text{d}}}{2(r^2 + r_{\text{c}}^2)^2}, \quad (11)$$

where the static dipole polarizability of the water molecule $\alpha_{\text{d}} = 9.7949$ a.u. [30] and r_{c} is the cutoff parameter proposed by Mittleman and Watson [31]:

$$r_{\text{c}} = \left[\frac{1}{2} \alpha_{\text{d}} z^{-1/3} b_{\text{pol}}^2 \right]^{1/4}, \quad (12)$$

with $z = 10$ and b_{pol} an adjustable parameter given by:

$$b_{\text{pol}} = \sqrt{\max\{(E - 0.5)/0.01; 1\}}. \quad (13)$$

The correlation potential differs for electrons and positrons and has been well described by Padiál and Norcross [32] for the former and by Jain [33] for the latter. The corresponding expressions $V_{\text{corr}}^-(r)$ and $V_{\text{corr}}^+(r)$ are reported below:

$$\begin{cases} V_{\text{corr}}^-(r_{\text{s}}) = 0.0311 \ln r_{\text{s}} - 0.0584 + 0.006 r_{\text{s}} \ln r_{\text{s}} \\ \quad - 0.015 r_{\text{s}} & \text{for } r_{\text{s}} \leq 0.7, \\ V_{\text{corr}}^-(r_{\text{s}}) = -0.07356 + 0.02224 \ln r_{\text{s}} & \text{for } 0.7 \leq r_{\text{s}} \leq 10, \\ V_{\text{corr}}^-(r_{\text{s}}) = -0.584 r_{\text{s}}^{-1} + 1.988 r_{\text{s}}^{-3/2} - 2.450 r_{\text{s}}^{-2} \\ \quad - 0.733 r_{\text{s}}^{-5/2} & \text{for } r_{\text{s}} \geq 10, \end{cases} \quad (14)$$

with $r_{\text{s}} = \left[\frac{3}{4\pi\rho(r)} \right]^{1/3}$ and:

$$\begin{cases} V_{\text{corr}}^+(r_{\text{s}}) = \frac{1}{2} \left\{ -\frac{1.82}{r_{\text{s}}^{1/2}} + (0.051 \ln r_{\text{s}} - 0.115) \ln r_{\text{s}} \right. \\ \quad \left. + 1.167 \right\} & \text{for } r_{\text{s}} \leq 0.302, \\ V_{\text{corr}}^+(r_{\text{s}}) = \frac{1}{2} \left\{ -0.92305 - \frac{0.09098}{r_{\text{s}}^2} \right\} & \text{for } 0.302 \leq r_{\text{s}} \leq 0.56, \\ V_{\text{corr}}^+(r_{\text{s}}) = \frac{1}{2} \left\{ -\frac{8.7674 r_{\text{s}}}{(r_{\text{s}}+2.5)^3} + \frac{-13.151+0.9552 r_{\text{s}}}{(r_{\text{s}}+2.5)^2} \right. \\ \quad \left. + \frac{2.8655}{r_{\text{s}}+2.5} - 0.6298 \right\} & \text{for } 0.56 \leq r_{\text{s}} \leq 8.0. \end{cases} \quad (15)$$

Finally, the exchange effect (only used for electrons) was treated via the phenomenological potential $V_{\text{ex}}(r)$ proposed by Riley and Truhlar [34], and is expressed as

$$V_{\text{ex}}(r) = \frac{1}{2} \left\{ \begin{aligned} &E_{\text{inc}} - (V_{\text{st}}(r) + V_{\text{cp}}(r)) \\ &- \left[(E_{\text{inc}} - (V_{\text{st}}(r) + V_{\text{cp}}(r)))^2 + 4\pi\rho(r) \right]^{1/2} \end{aligned} \right\}. \quad (16)$$

Ionization. In the case of ionization, the kinetic energy of the ejected electron E_e is first determined by random sampling among the singly differential cross sections. Then by applying a direct MC sampling according to the relative magnitude of the partial total ionization cross sections (at E_e), the ionization potential IP_j is determined. The particle energy is reduced by $E_e + IP_j$, whereas the ejected and scattered directions are determined according to the triply and double differential cross sections, respectively. The particular ionization potential IP_j is stored as locally deposited energy, except when inner-shell ionization occurs, in which case an Auger electron is produced and assumed to be isotropically emitted with a kinetic energy E_{Auger} [7, 12].

Regarding the theoretical approach, the ionization process is described within the frozen-core first Born approximation that consists in reducing the ten-electron problem to a one active electron problem (for more details see [35]). Thus, the triply differential cross sections (TDCS) are defined as

$$\sigma^{(3)}(\Omega_s, \Omega_e, E_e) \equiv \frac{d^3\sigma_j}{d\Omega_s d\Omega_e dE_e} = \frac{k_e k_s}{k_i} |M|^2, \quad (17)$$

where $d\Omega_s = \sin\theta_s d\theta_s d\phi_s$ and $d\Omega_e = \sin\theta_e d\theta_e d\phi_e$ correspond to the scattered and ejected direction, respectively. The momenta \mathbf{k}_i , \mathbf{k}_s and \mathbf{k}_e are related to the incident, the scattered and the ejected electron, respectively. The transition amplitude M is given by

$$M = \frac{1}{2\pi} \langle \Psi_f | V | \Psi_i \rangle, \quad (18)$$

where V represents the interaction between the incident electron and the target and is written as

$$V = -\frac{8}{r_0} - \frac{1}{|\mathbf{r}_0 - \mathbf{R}_1|} - \frac{1}{|\mathbf{r}_0 - \mathbf{R}_2|} + \sum_{i=1}^{10} \frac{1}{|\mathbf{r}_0 - \mathbf{r}_i|}, \quad (19)$$

with $R_1 = R_2 = R_{\text{OH}} = 1.814$ a.u., while \mathbf{r}_i is the position of the i th bound electron of the target with respect to the oxygen nucleus [36]. The initial state is written as the product of two wave functions: a first one $\phi(\mathbf{k}_i, \mathbf{r}_0)$ describing the incident electron by a plane wave and a second one $\varphi_i(\mathbf{r}_1, \mathbf{r}_2, \dots, \mathbf{r}_{10})$ for the ten bound electrons described by the Slater functions given by Moccia. Thus, the initial state is expressed as

$$|\Psi_i\rangle = |\phi(\mathbf{k}_i, \mathbf{r}_0) \varphi_i(\mathbf{r}_1, \mathbf{r}_2, \dots, \mathbf{r}_{10})\rangle. \quad (20)$$

Considering the final state of the collisional system, it was successively described within five different models: two first models where the incident and the scattered electrons are both described by plane waves, whereas the ejected one is described by a Coulomb wave (FBA-CW) or a distorted wave (DWBA), respectively; a two-Coulomb wave (2CW) model where the scattered and ejected electrons are both described by a Coulomb wave; the Branner, Briggs, and Klar (BBK) model whose main characteristic consists of exhibiting a correct asymptotical Coulomb three-body wave function for the ejected and scattered electrons in the residual ion field and finally the DS3C—for dynamic screening of the three two-body Coulomb model. For more details about these models as well as a fine analysis of the respective improvements, we refer the reader to our previous work [36]. However, on the basis of TDCS calculations and comparisons with available experimental measurements, we concluded that the two first-order models, namely, FBA-CW and DWBA, reproduced quite well the shape of the TDCS, the 2CW model giving nevertheless a better agreement with experiments than the first cited ones, even considering that the recoil peak remains still underestimated for some molecular orbitals. Considering the double structure of the binary region, it is generally well reproduced for all models. However, we observed that none of the models—even the rather sophisticated DS3C approach—reproduces correctly the data at low ejection angles. To conclude, for computational time reasons, we first focused our efforts to the building and the implementation in CELLDOSE of a DWBA database including triply, doubly, singly differential, and total cross sections.

Let us remind that the water target wave function used here refers to an *isolated* water molecule, namely, in *vapor* phase. For a more realistic modeling of the electron tracking in biological matter, it is worth noting that water should be considered in its liquid phase. To that end, various semi-empirical models were developed since the pioneer works of the Oak Ridge group [37,38]. For more details, we refer the reader to the works of Emfietzoglou and coworkers [39–41]. In this context, we reported in a recent work [25] a unified methodology to express the molecular wave functions of water in the liquid phase by means of a single center approach and reported a low influence of the water phase on the cross section calculations, limited to the low-incident energy regime. Indeed, in this energy range, the contribution of the outermost target subshells to the ionization cross sections is very important, which leads to an increasing influence of the water phase as the incident electron energy decreases.

Excitation. When the selected interaction is excitation, direct MC sampling is applied according to the relative magnitude of all partial excitation cross sections for determining the excitation level n . The particle energy is reduced by the potential energy W_n , assumed as locally deposited, whereas the incident direction remains unaltered [7].

Excitation includes all the processes which modify the internal state of the molecule without emission of electrons. These processes include, in particular, the following:

1. Electronic transitions toward Rydberg states or degenerate states (\tilde{A}_1B_1 , \tilde{B}_1A_1 , diffuse band);
2. The dissociative excitation processes leading to excited radicals (H^* , O^* , and OH^*);
3. The vibrational and rotational channels;
4. The dissociative attachment leading to the formation of negative ions.

It is worth noting that describing the electronic states of molecular targets remains a challenging task in a quantum-mechanical approach. In this context, we first privileged semi-empirical models for treating both the electron- and positron-induced excitations. For the first three processes listed above, the total excitation cross sections are given by [11, 42, 43]

$$\sigma_n(E_{\text{inc}}) = \frac{4\pi a_0^2 R y^2 f_0^{(n)} c_0^{(n)}}{W_n^2} \left(\frac{W_n}{E_{\text{inc}}} \right)^\Omega \left[1 - \left(\frac{W_n}{E_{\text{inc}}} \right)^\beta \right]^\nu, \quad (21)$$

where W_n is the deposited energy during the excitation channel labeled n , and Ω , β , ν are fitting parameters; $f_0^{(n)}$ and $c_0^{(n)}$ being the oscillator strength and a constant of normalization deduced from experimental total cross sections $\sigma_n(E_{\text{inc}})$, respectively. All these parameters are listed in Olivero et al. [42]. For the dissociative attachment process, the following expression is used [44]:

$$\sigma_n(E_{\text{inc}}) = \frac{Ae^t}{U(1+e^t)^2} \quad (22)$$

with:

$$t = \frac{E_{\text{inc}} - W_n}{U}, \quad (23)$$

where A and U are fitting parameters. Moreover, let us add that according to experimental results [44], we assume that impact excitation induces no angular deflection.

Positronium Formation. When the incident particle is a positron, a target electron capture process can take place, leading in the final channel of the reaction to the formation of Positronium atoms (Ps), a bound system consisting of an electron and a positron. In its ground state (triplet state), this exotic system has a mean lifetime of approximately 1.47×10^{-7} s (ortho-Positronium) annihilating in three photons, whereas in the singlet state (para-Positronium) its mean lifetime is approximately 1.25×10^{-10} s with annihilation in two photons of 511 keV each, the rest mass of the electron. The knowledge of this process is important for many domains of physics as well as in medicine, a field where it is nowadays common the use of positron emission tomography (PET) for both diagnostic and treatment monitoring.

The description of the Positronium formation process when positrons collide with a water target is based on the work by Hervieux et al. [45], who developed a continuum distorted-wave final state (CDW-FS) approximation. Within

this approach, the final state of the collision is distorted by two-Coulomb wave functions associated with the interaction of both the positron and the active electron (the captured one) with the residual ionic target. Since the collision of a positron with a vapor water molecule is a many-electron problem, the independent electron model (IEM) was adopted. This means that at the high impact energies considered here, it is possible to assume that the electron is, before being captured, suddenly ejected into an intermediate state corresponding to a high-velocity continuum of the target (with a velocity close to the projectile one). Therefore, it is considered that the other electrons remain as frozen in their initial orbitals due to the fact that the relaxation time is much larger than the collision one. The total cross sections are calculated by using a partial-wave technique. More details are given in [45].

2.3 Future Developments

The next step in the development of CELLDOSE is to extend the code by including the interactions of heavier charged particles, namely protons and alpha particles, with water and DNA. This will be achieved by coupling CELLDOSE with TILDA-V (an acronym for “Transport d’Ions Lourds Dans l’Aqua & Vivo”), a newly developed MCTS code [6, 46]. In its current version, TILDA-V is able to simulate the full transport of protons and its secondaries in water and DNA components. Thus, the main task remains the modeling of alpha particles, taking into account all the charge states of the helium atom [47, 48]. With the growing interest in targeted alpha therapy (TAT) for treating microscopic or small-volume disease [49], an accurate nano-dosimetric description of the pattern of energy deposit of alpha particles could be a valuable input to assess and compare the potential therapeutical advantages of several alpha-emitting radionuclides. This is even more true given that microdosimetry seems essential to investigate the therapeutic efficacy of TAT [50].

3 Results

We present here some recent results obtained with the latest version of CELLDOSE. We have computed the stopping power and penetration range for electrons in water and DNA for incident energies, E_{inc} in the range 10 eV to 10^4 eV. To compute the stopping power one million histories of stationary projectiles, i.e., primary particles for which the initial energy remains unchanged, were simulated. In this mode, each primary particle is followed until it experiences an interaction with the medium. A sum over the energy loss and the distance traveled by each particle is carried out and the linear stopping power—expressed in $\text{keV } \mu\text{m}^{-1}$ —is then defined as

$$SP = \frac{E_{tot}}{L}, \quad (24)$$

where E_{tot} is the total energy lost by the stationary projectiles and L is the track length. The results were later normalized using the mass densities for

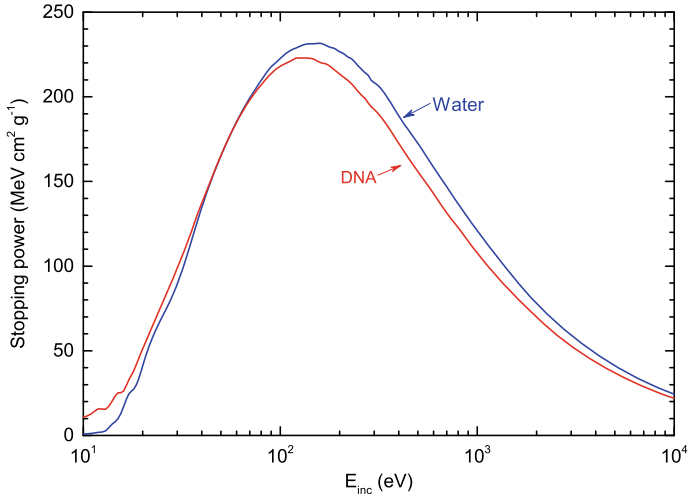


Fig. 1. Total stopping power for electrons in water versus DNA as provided by CELLDOSE

each medium ($\rho_{\text{H}_2\text{O}} = 1 \text{ g cm}^{-3}$, $\rho_{\text{DNA}} = 1.29 \text{ g cm}^{-3}$ [19]) to obtain the mass stopping power, expressed in $\text{MeV cm}^2 \text{ g}^{-1}$. Figure 1 represents the total stopping power for electrons in water versus DNA. The results display a similar behavior for both media, with a maximum stopping power of $232 \text{ MeV cm}^2 \text{ g}^{-1}$ at 160 eV and $223 \text{ MeV cm}^2 \text{ g}^{-1}$ at 120 eV for water and DNA, respectively. It is worth noting that the linear stopping power of DNA is greater than for water; however, when normalizing with respect to the mass density of the medium to obtain the mass stopping power as mentioned before, the DNA curve initially above the one from water is shifted downwards, as shown in Fig. 1.

Figure 2 shows the contribution of ionization as well as excitation processes to the total stopping power of electrons in both media. In panel (a) we report our results for water and compare them with values found in the literature. A good agreement can be seen with the data provided in the IAEA TECDOC 799 [51] and the ICRU Report 16 [52] for $E_{\text{inc}} > 300 \text{ eV}$, as well as with the calculations by Garcia-Molina et al. [53] and Tan et al. [54] for $E_{\text{inc}} > 500 \text{ eV}$. At lower energies, however, important discrepancies are observed, especially with respect to the maximum value of the stopping power, since there is a difference of about 12% and 19% between our values and the predictions of Garcia-Molina et al. [53] and Tan et al. [54], respectively. This can be explained by the fact that both authors used the dielectric formalism for their calculations, which without all the necessary corrections is known to overestimate the inelastic cross sections at the peak region, as pointed out in the work by Tan et al. [54]. Finally, our predictions agree with the results obtained by Paretzke [55] in most of the energy range here considered, although a slight underestimation of the maximum is still noticeable. Panel (b) shows our results for DNA. As in the case of water, significant dif-

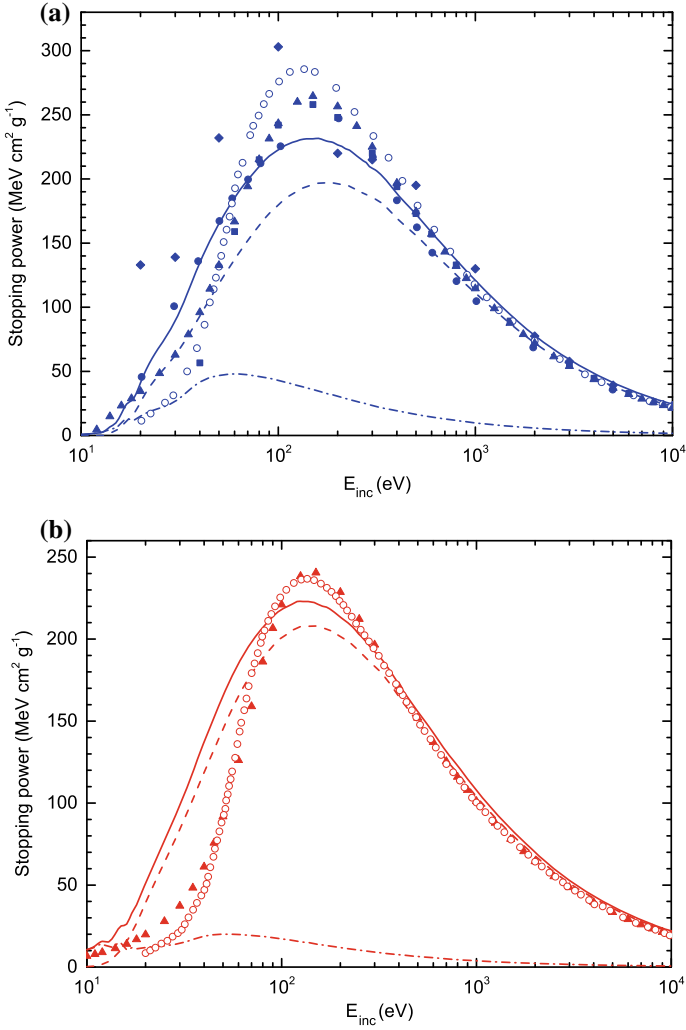


Fig. 2. Contribution of ionization and excitation processes (dashed and dash-dotted line, respectively) to the total stopping power for electrons in **a** water and **b** DNA (blue and red solid lines, respectively), as provided by CELLDOSE. Total stopping power data are taken from the IAEA TECDOC 799 [51] (squares), the ICRU report 16 [52] (diamonds), Garcia-Molina et al. [53] (triangles), Tan et al. [54] (open circles) and Paretzke [55] (solid circles)

ferences are observed between our values and those of Garcia-Molina et al. [53] and Tan et al. [54] at low energies and near the peak region. Nevertheless, now the maximum stopping power values predicted by Garcia-Molina et al. [53] and Tan et al. [54] are only 7% and 6% greater than our result, respectively. On the

other hand, a good agreement between the three calculations can be observed for $E_{\text{inc}} > 300$ eV.

Figure 3 presents our results for the penetration range of electrons in water and DNA (blue and red solid line, respectively). We apply here the same definition of penetration range used by Meesungnoen et al. [56], namely, the length of the vector $|\mathbf{R}_f - \mathbf{R}_i|$ from the point of departure (\mathbf{R}_i) to the final position (\mathbf{R}_f) of the electron after thermalization. As shown in Fig. 3, at energies below ~ 700 eV our results for water fall between those of Meesungnoen et al. [56] (open circles) and the values computed with the default version of Geant4-DNA [57] (solid diamonds). For incident energies above ~ 700 eV the three predictions overlap perfectly. The penetration range for electrons in DNA is represented in Fig. 3 by the red solid line. It can be observed that in the whole energy range here considered the penetration range values for DNA are lower than those for water. There is a maximum difference of 80% in the penetration range for both media at 10 eV, while for energies higher than 2 keV the difference falls to about 15%. In order to confirm that this behavior is not only due to the different densities considered for water and DNA, we have plotted in Fig. 4 the penetration range in water with the density rescaled to a value of 1.29 g cm^{-3} (blue dashed line). The results show that even after the density correction the difference in the penetration range for electrons in water and DNA is still remarkable at low incident energies, reaching 75% at 10 eV. On the other hand, it can be seen that at about 500 eV the penetration range is almost the same for both media. At

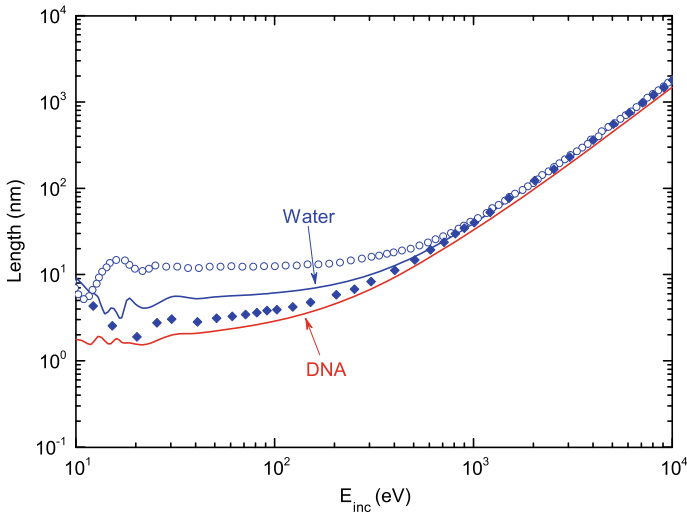


Fig. 3. Penetration range for electrons in water (blue solid line) and DNA (red solid line), as provided by CELLDOSE. Calculations provided by Meesungnoen et al. [56] (open circles) and results obtained with the default version of Geant4-DNA, as reported by Bordage et al. [57] (solid diamonds), are shown for comparison

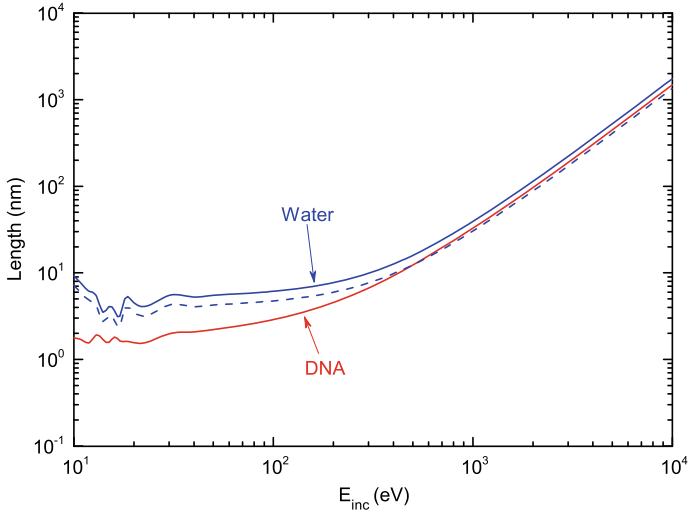


Fig. 4. Penetration range for electrons in water (blue solid line), water with the density rescaled to 1.29 g cm^{-3} (blue dashed line) and DNA (red solid line), as provided by CELLDOSE

higher impact energies ($E_{\text{inc}} > 500 \text{ eV}$), the penetration range in DNA becomes greater than in density-rescaled water, with a difference of about 9% at 10 keV.

4 Conclusion

We have reviewed in this paper the main features and physical models implemented in the CELLDOSE MCTS code. We have also presented our latest calculations regarding the stopping power and penetration range for electrons in water and DNA, showing that for the former medium our results are in agreement with the values found in the literature. In the case of DNA we have provided here the predictions of our code and compared our stopping power values with the calculations performed by other authors, observing differences at low incident energies and a better agreement for $E_{\text{inc}} > 300 \text{ eV}$. Our results could be taken as a reference for future comparisons as more experimental data and theoretical calculations on this medium become available. Finally, we have briefly discussed the objectives of the ongoing work to improve and extend our code, underlining the significant potential applications in ionizing radiation microdosimetry and targeted alpha therapy.

References

1. Nikjoo, H., Uehara, S., Emfietzoglou, D., Cucinotta, F.A.: Track-structure codes in radiation research. *Radiat. Meas.* **41**, 1052–1074 (2006). <https://doi.org/10.1016/j.radmeas.2006.02.001>

2. Nikjoo, H., Emfietzoglou, D., Liamsuwan, T., Taleei, R., Liljequist, D., Uehara, S.: Radiation track, DNA damage and response-a review. *Rep. Prog. Phys.* **79**, 116601 (2016). <https://doi.org/10.1088/0034-4885/79/11/116601>
3. Kyriakou, I., Emfietzoglou, D., Ivanchenko, V., Bordage, M.C., Guatelli, S., Lazarakis, P., Tran, H.N., Incerti, S.: Microdosimetry of electrons in liquid water using the low-energy models of Geant4. *J. Appl. Phys.* **122**, 024303 (2017). <https://doi.org/10.1063/1.4992076>
4. Nikjoo, H., Taleei, R., Liamsuwan, T., Liljequist, D., Emfietzoglou, D.: Perspectives in radiation biophysics: from radiation track structure simulation to mechanistic models of DNA damage and repair. *Radiat. Phys. Chem.* **128**, 3–10 (2016). <https://doi.org/10.1016/j.radphyschem.2016.05.005>
5. Friedland, W., Dingfelder, M., Kunderát, P., Jacob, P.: Track structures, DNA targets and radiation effects in the biophysical Monte Carlo simulation code PAR-TRAC. *Mutat. Res. Fund Mol. Mech. Mutagen.* **711**, 28–40 (2011). <https://doi.org/10.1016/j.mrfmmm.2011.01.003>
6. Quinto, M.A., Monti, J.M., Weck, P.F., Fojón, O.A., Hanssen, J., Rivarola, R.D., Senot, P., Champion, C.: Monte Carlo simulation of proton track structure in biological matter. *Eur. Phys. J. D* **71**, 130 (2017). <https://doi.org/10.1140/epjd/e2017-70709-6>
7. Champion, C., Zanotti-Fregonara, P., Hindíé, E.: CELLDOSE: a Monte Carlo code to assess electron dose distribution S values for ^{131}I in spheres of various sizes. *J. Nucl. Med.* **49**, 151–157 (2007). <https://doi.org/10.2967/jnumed.107.045179>
8. Champion, C., Hanssen, J., Hervieux, P.A.: Electron impact ionization of water molecule. *J. Chem. Phys.* **117**, 197–204 (2002). <https://doi.org/10.1063/1.1472513>
9. Aouchiche, H., Champion, C., Oubaziz, D.: Electron and positron elastic scattering in gaseous and liquid water: a comparative study. *Radiat. Phys. Chem.* **77**, 107–114 (2008). <https://doi.org/10.1016/j.radphyschem.2007.09.004>
10. Champion, C.: Quantum-mechanical predictions of electron-induced ionization cross sections of DNA components. *J. Chem. Phys.* **138**, 184306 (2013). <https://doi.org/10.1063/1.4802962>
11. Champion, C.: Theoretical cross sections for electron collisions in water: structure of electron tracks. *Phys. Med. Biol.* **48**, 2147–2168 (2003). <https://doi.org/10.1088/0031-9155/48/14/308>
12. Champion, C., Le Loirec, C., Stosic, B.: EPOTRAN: a full-differential Monte Carlo code for electron and positron transport in liquid and gaseous water. *Int. J. Radiat. Biol.* **88**, 54–61 (2012). <https://doi.org/10.3109/09553002.2011.641451>
13. Champion, C., Quinto, M.A., Morgat, C., Zanotti-Fregonara, P., Hindíé, E.: Comparison between three promising β -emitting radionuclides, ^{67}Cu , ^{47}Sc and ^{161}Tb , with emphasis on doses delivered to minimal residual disease. *Theranostics* **6**, 1611–1618 (2016). <https://doi.org/10.7150/thno.15132>
14. Hindíé, E., Champion, C., Zanotti-Fregonara, P., Rubello, D., Colas-Linhart, N., Ravasi, L., Moretti, J.-L.: Calculation of electron dose to target cells in a complex environment by Monte Carlo code “CELLDOSE”. *Eur. J. Nucl. Med. Mol. Imaging* **36**, 130–136 (2009). <https://doi.org/10.1007/s00259-008-0893-z>
15. Moccia, R.: One-center basis set SCF MO's. III. H_2O , H_2S , and HCL . *J. Chem. Phys.* **40**, 2186–2192 (1964). <https://doi.org/10.1063/1.1725491>
16. Frisch, M.J., et al.: Gaussian 09, Revision A.02. Gaussian, Inc., Wallingford, CT (2009)
17. Galassi, M.E., Champion, C., Weck, P.F., Rivarola, R.D., Fojón, O., Hanssen, J.: Quantum-mechanical predictions of DNA and RNA ionization by energetic

- proton beams. *Phys. Med. Biol.* **57**, 2081–2099 (2012). <https://doi.org/10.1088/0031-9155/57/7/2081>
18. Tan, Z., Xia, Y., Zhao, M., Liu, X.: Proton stopping power in a group of bioorganic compounds over the energy range of 0.05–10 MeV. *Nucl. Instrum. Methods B* **248**, 1–6 (2006). <https://doi.org/10.1016/j.nimb.2006.04.073>
 19. Birnie, G.D., Rickwood, D., Hell, A.: Buoyant densities and hydration of nucleic acids, proteins and nucleoprotein complexes in metrizamide. *Biochim. Biophys. Acta* **331**, 283–294 (1973). [https://doi.org/10.1016/0005-2787\(73\)90441-3](https://doi.org/10.1016/0005-2787(73)90441-3)
 20. Dingfelder, M., Inokuti, M., Paretzke, H.G.: Inelastic-collision cross sections of liquid water for interactions of energetic protons. *Radiat. Phys. Chem.* **59**, 255–275 (2000). [https://doi.org/10.1016/S0969-806X\(00\)00263-2](https://doi.org/10.1016/S0969-806X(00)00263-2)
 21. Abril, I., Garcia-Molina, R., Denton, C.D., Kyriakou, I., Emfietzoglou, D.: Energy loss of hydrogen- and helium-ion beams in DNA: calculations based on a realistic energy-loss function of the target. *Radiat. Res.* **175**, 247–255 (2011)
 22. de Vera, P., Garcia-Molina, R., Abril, I.: Angular and energy distributions of electrons produced in arbitrary biomaterials by proton impact. *Phys. Rev. Lett.* **114**, 018101 (2015). <https://doi.org/10.1103/PhysRevLett.114.018101>
 23. Emfietzoglou, D., Karava, K., Papamichael, G., Moscovitch, M.: Monte Carlo simulation of the energy loss of low-energy electrons in liquid water. *Phys. Med. Biol.* **48**, 2355–2371 (2003). <https://doi.org/10.1088/0031-9155/48/15/308>
 24. Blanco, F., Roldán, A.M., Krupa, K., McEachran, R.P., White, R.D., Marjanović, S., Petrović, Z.L., Brunger, M.J., Machacek, J.R., Buckman, S.J., Sullivan, J.P., Chiari, L., Limão-Vieira, P., García, G.: Scattering data for modelling positron tracks in gaseous and liquid water. *J. Phys. B At. Mol. Opt. Phys.* **49**, 145001 (2016). <https://doi.org/10.1088/0953-4075/49/14/145001>
 25. Champion, C.: Electron impact ionization of liquid and gaseous water: a single-center partial-wave approach. *Phys. Med. Biol.* **55**, 11–32 (2010). <https://doi.org/10.1088/0031-9155/55/1/002>
 26. Neufeind, J., Benmore, C.J., Tomberli, B., Egelstaff, P.A.: Experimental determination of the electron density of liquid H₂O and D₂O. *J. Phys. Condens. Matter* **14**, L429–L433 (2002). <https://doi.org/10.1088/0953-8984/14/23/104>
 27. Ichikawa, K., Kameda, Y., Yamaguchi, T., Wakita, H., Misawa, M.: Neutron-diffraction investigation of the intramolecular structure of a water molecule in the liquid phase at high temperatures. *Mol. Phys.* **73**, 79–86 (1991). <https://doi.org/10.1080/00268979100101071>
 28. Moriarty, N.W., Karlström, G.: Geometry optimization of a water molecule in water. A combined quantum chemical and statistical mechanical treatment. *J. Chem. Phys.* **106**, 6470–6474 (1997). <https://doi.org/10.1063/1.473637>
 29. Salvat, F.: Optical-model potential for electron and positron elastic scattering by atoms. *Phys. Rev. A* **68**, 012708 (2003). <https://doi.org/10.1103/PhysRevA.68.012708>
 30. Jain, A., Thompson, D.G.: Elastic scattering of slow electrons by CH₄ and H₂O using a local exchange potential and new polarisation potential. *J. Phys. B At. Mol. Phys.* **15**, L631–L637 (1982). <https://doi.org/10.1088/0022-3700/15/17/012>
 31. Mittleman, M.H., Watson, K.M.: Effects of the Pauli principle on the scattering of high-energy electrons by atoms. *Ann. Phys.* **10**, 268–279 (1960) (New York). [https://doi.org/10.1016/0003-4916\(60\)90024-5](https://doi.org/10.1016/0003-4916(60)90024-5)
 32. Padiál, N.T., Norcross, D.W.: Parameter-free model of the correlation-polarization potential for electron-molecule collisions. *Phys. Rev. A* **29**, 1742–1748 (1984). <https://doi.org/10.1103/PhysRevA.29.1742>

33. Jain, A.: Low-energy positron-argon collisions by using parameter-free positron correlation polarization potentials. *Phys. Rev. A* **41**, 2437–2444 (1990). <https://doi.org/10.1103/PhysRevA.41.2437>
34. Riley, M.E., Truhlar, D.G.: Approximations for the exchange potential in electron scattering. *J. Chem. Phys.* **63**, 2182–2191 (1975). <https://doi.org/10.1063/1.431598>
35. Champion, C., Hanssen, J., Rivarola, R.D.: The first born approximation for ionization and charge transfer in energetic collisions of multiply charged ions with water. In: *Advances in Quantum Chemistry*. Elsevier, pp. 269–313 (2013). <https://doi.org/10.1016/B978-0-12-396455-7.00010-8>
36. Champion, C., Cappello, C.D., Houamer, S., Mansouri, A.: Single ionization of the water molecule by electron impact: angular distributions at low incident energy. *Phys. Rev. A* **73**, 012717 (2006). <https://doi.org/10.1103/PhysRevA.73.012717>
37. Ritchie, R.H., Hamm, R.N., Turner, J.E., Wright, H.A.: The interaction of swift electrons with liquid water. In: *6th Symposium on Microdosimetry*, pp. 345–354. Harwood Academic, London (1978)
38. Ashley, J.C.: Stopping power of liquid water for low-energy electrons. *Radiat. Res.* **89**, 25–31 (1982). <https://doi.org/10.2307/3575681>
39. Emfietzoglou, D.: Inelastic cross-sections for electron transport in liquid water: a comparison of dielectric models. *Radiat. Phys. Chem.* **66**, 373–385 (2003). [https://doi.org/10.1016/S0969-806X\(02\)00504-2](https://doi.org/10.1016/S0969-806X(02)00504-2)
40. Emfietzoglou, D., Cucinotta, F.A., Nikjoo, H.: A complete dielectric response model for liquid water: a solution of the bethe ridge problem. *Radiat. Res.* **164**, 202–211 (2005). <https://doi.org/10.1667/RR3399>
41. Emfietzoglou, D., Nikjoo, H.: Accurate electron inelastic cross sections and stopping powers for liquid water over the 0.1–10 keV range based on an improved dielectric description of the Bethe surface. *Radiat. Res.* **167**, 110–120 (2007). <https://doi.org/10.1667/RR0551.1>
42. Olivero, J.J., Stagat, R.W., Green, A.E.S.: Electron deposition in water vapor, with atmospheric applications. *J. Geophys. Res.* **77**, 4797–4811 (1972). <https://doi.org/10.1029/JA077i025p04797>
43. Green, A.E.S., Dutta, S.K.: Semi-empirical cross sections for electron impacts. *J. Geophys. Res.* **72**, 3933–3941 (1967). <https://doi.org/10.1029/JZ072i015p03933>
44. Compton, R.N., Christophorou, L.G.: Negative-ion formation in H₂O and D₂O. *Phys. Rev.* **154**, 110–116 (1967). <https://doi.org/10.1103/PhysRev.154.110>
45. Hervieux, P.-A., Fojón, O.A., Champion, C., Rivarola, R.D., Hanssen, J.: Positronium formation in collisions of fast positrons impacting on vapour water molecules. *J. Phys. B. At. Mol. Opt.* **39**, 409–419 (2006). <https://doi.org/10.1088/0953-4075/39/2/015>
46. Quinto, M.A., Monti, J.M., Galassi, M.E., Weck, P.F., Fojón, O.A., Hanssen, J., Rivarola, R.D., Champion, C.: Proton track structure code in biological matter. *J. Phys. Conf. Ser.* **583**, 012049 (2015). <https://doi.org/10.1088/1742-6596/583/1/012049>
47. Garcia-Molina, R., Abril, I., Heredia-Avalos, S., Kyriakou, I., Emfietzoglou, D.: A combined molecular dynamics and Monte Carlo simulation of the spatial distribution of energy deposition by proton beams in liquid water. *Phys. Med. Biol.* **56**, 6475–6493 (2011). <https://doi.org/10.1088/0031-9155/56/19/019>
48. Liamsuwan, T., Uehara, S., Emfietzoglou, D., Nikjoo, H.: Physical and biophysical properties of proton tracks of energies 1 keV to 300 MeV in water. *Int. J. Radiat. Biol.* **87**, 141–160 (2011). <https://doi.org/10.3109/09553002.2010.518204>

49. Mulford, D.A., Scheinberg, D.A., Jurcic, J.G.: The promise of targeted α -particle therapy. *J. Nucl. Med.* **46**, 199S–204S (2005)
50. Huang, C.-Y., Guatelli, S., Oborn, B.M., Allen, B.J.: Microdosimetry for targeted alpha therapy of cancer. *Comput. Math. Methods Med.* **2012**, 1–6 (2012). <https://doi.org/10.1155/2012/153212>
51. International Atomic Energy Agency: Atomic and Molecular Data for Radiotherapy and Radiation Research IAEA-TECDOC-799. IAEA, Vienna (1995)
52. International Commission on Radiation Units and Measurements: ICRU Report 16 Linear Energy Transfer. ICRU, Bethesda, MD (1970)
53. Garcia-Molina, R., Abril, I., Kyriakou, I., Emfietzoglou, D.: Inelastic scattering and energy loss of swift electron beams in biologically relevant materials: energy loss of electron beams in biomaterials. *Surf. Interface Anal.* **49**, 11–17 (2017). <https://doi.org/10.1002/sia.5947>
54. Tan, Z., Xia, Y., Zhao, M., Liu, X.: Electron stopping power and inelastic mean free path in amino acids and protein over the energy range of 20–20,000 eV. *Radiat. Environ. Biophys.* **45**, 135–143 (2006). <https://doi.org/10.1007/s00411-006-0049-0>
55. Paretzke, H.G.: Simulation von Elektronenspuren im Energiebereich 0.01–10 keV in Wasserdampf. Report No. 24/88, GSF—National Research Center for Health and Environment (1988)
56. Meesungnoen, J., Filali-Mouhim, A., Mankhetkorn, S.: Low-energy electron penetration range in liquid water. *Radiat. Res.* **158**, 657–660 (2002)
57. Bordage, M.C., Bordes, J., Edel, S., Terrissol, M., Franceries, X., Bardiès, M., Lampe, N., Incerti, S.: Implementation of new physics models for low energy electrons in liquid water in Geant4-DNA. *Phys. Med.* **32**, 1833–1840 (2016). <https://doi.org/10.1016/j.ejmp.2016.10.006>